LATERAL VERSUS LONGITUDINAL ARTIFICIAL
REEF SYSTEMS

Yoshimi Goda[1] and Hiroshi Takagi[2]

Abstract

A new submerged breakwater structure for shore protection is proposed and called the longitudinal reef system. It is efficient in dissipating wave energy by increasing wave heights at the front through wave refraction effect and by enhancing wave breaking. Comparison is made between the new longitudinal reef system and the conventional broad-crested reef system through model experiments and numerical computation. The superiority of the longitudinal system to the conventional system is confirmed through the comparison.

Introduction

Shore-parallel, detached breakwaters have been used in many countries to protect beaches from erosion. As their emerged crests obstruct the aesthetic view of the sea from beach areas, however, they are sometimes rejected by local residents and visitors. Thus, submerged breakwaters with broad crests are developed and built at several coasts around Japan; they are called artificial reefs.

Artificial reefs dissipate incoming wave energy by forcing them to break on top of the crests because of shallow depth there. Energy dissipation could be enhanced if the wave refraction effect is mobilized to increase wave heights before breaking. This can be done by building a number of slender artificial reefs arranged longitudinally as shown in Fig. 1. Goda (1995) named such a system as a longitudinal reef system. The conventional artificial reefs with crests extended alongshore are called the lateral artificial reefs in the present paper.

In the previous paper by Goda (1995), wave transmission characteristics over a longitudinal reef system were presented, based on wave flume tests and numerical computations. The present paper discusses the results of 3-D tests in a wave

[1] Professor, [2] Graduate Student, Yokohama National University, Department of Civil Engineering, 79-5 Tokiwadai, Hodogaya-ku, Yokohama 240-8501, Japan
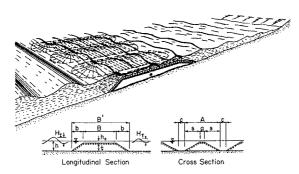
Fig. 1 Sketch of longitudinal artificial reef system.

basin for wave heights and wave-induced currents around both lateral and longitudinal reef systems, and compares their performances by means of numerical computations.

Models of Longitudinal and Lateral Reef Systems for Tests

Volume of Reef Unit

With the notations listed in Fig. 1, the volume of one unit of reefs is approximately calculated by Eq. 1.

$$V = t[b(a + \pi s/3) + (a + s)B] \tag{1}$$

The above equation applies for both lateral and longitudinal reef systems; *i.e.*, the former has the crest width a greater than the crest length B, while the latter has a smaller than B.

In the comparison between the lateral and longitudinal reef systems, their construction cost is an important factor together with their hydrodynamic characteristics. As the construction cost is primarily controlled by the total volume of reef units, model reefs of longitudinal and lateral units were built with the same total volume to make a fair comparison of their performance.

Wave Basin for Model Tests

An outdoor wave basin with the size of 9.0 m by 13.0 m was employed in the present study. A planar slope with the inclination of 1/20 was built with mortar in a slant angle of 15° to the wave paddles as shown in Fig. 2. The initial section of 0.52 m was made with the inclination of 1/10.

All the tests were carried out with the water depth of 0.30 m in front of the wave paddles. The grid lines of the x and y coordinates were drawn on the slope with the interval of 0.5 m with the origin at the upper left corner. The shoreline

was located at the line of $x = 6.0$ m. Two wave guide walls were placed at the both sides along the lines of refracted wave propagation; their locations were determined after several trials so as to insure smooth wave propagation along them.

Model Reef Units

Three longitudinal reef units were placed in the basin as shown in Fig. 2. The submergence depth was $h_c = 0.03$ m, the crest length was $B = 1.50$ m, and the crest width was $a = 0.10$ m. They were built with crushed stones with the diameters ranging from 30 to 50 mm. The front and rear slopes were $1/2$, and the side slope was $1/2.5$.
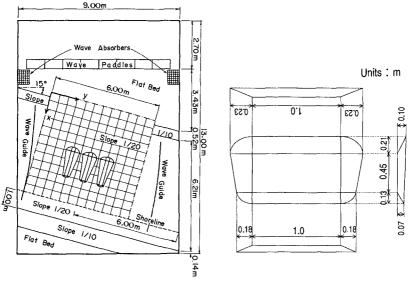

Fig. 2 Wave basin with longitudinal reefs.   Fig. 3 Sketch of a lateral reef unit.

These three longitudinal reef units were placed at the location of $x = 3.0$ to 4.5 m (crest position) with the separation of 1.0 m between the central axes which were located at $y = 2.0$, 3.0, and 4.0 m, respectively.

A lateral reef system was made with two units with $h_c = 0.03$ m, $B = 0.45$ m, and $a = 1.00$ m. Figure 3 provides a sketch of the lateral unit built on a slope of $1/20$. The total volumes of the longitudinal and lateral reef systems were about 0.127 m³ for both cases. The front line of the crests of two units were placed at the location of $x = 3.5$ m, and their central axes were set at the lines of $y = 2.1$ and 3.9 m.

Test Waves

Two trains of irregular waves with $H_{1/3}$ =7.5 cm and $T_{1/3}$ = 1.2 s and those with $H_{1/3}$ =5.5 cm and $T_{1/3}$ = 1.6 s were used in the tests. The offshore incident wave angle was 15°. Wave profiles were recorded with capacitance gauges at the sampling frequency of 20 Hz. The wave records were analyzed by the zero-downcrossing method, and the highest one-third wave height $H_{1/3}$ and period $T_{1/3}$ were computed. The data shown in the present paper refer to the significant wave height and period. Current velocities were measured with bi-axis ultrasonic current meters. Though the instrument could output instantaneous velocity data, only the mean currents averaged over 200 s were utilized for analysis of wave-induced currents.

Numerical Analysis of Wave Heights and Radiation Stresses

Governing Equation

Numerical simulation of wave deformation around the reef was made by using the parabolic equation based on the numerical scheme by Hirakuchi and Maruyama (1986). According to their scheme, the governing equation for the complex amplitude of the velocity potential, ϕ, is given as follows:

$$\frac{\partial \phi}{\partial x} = \left\{ i \left(k_x + \frac{k_y^2}{2k_x} \right) - \frac{1}{2k_x c c_g} \frac{\partial}{\partial x} (k_x c c_g) \right\} \phi + \frac{1}{2k_x c c_g} \frac{\partial}{\partial y} \left(c c_g \frac{\partial \phi}{\partial y} \right) - f_D' \phi \quad (2)$$

where k_x and k_y denotes the wave numbers in the x and y directions, respectively, c the wave celerity, c_g the group velocity, i the imaginary number. The term f_D' is a function which represents the effect of wave breaking on amplitude attenuation, and it is hereby called the wave attenuation function for brevity.

As the wave amplitude is proportional to the absolute amplitude of velocity potential, its spatial distribution is obtained by solving Eq. 2 with a forward difference scheme. Numerical computation was carried out for an area corresponding to physical model tests shown in Fig. 2: the grid size was set at $\Delta x = \Delta y = 0.10$ m.

Modification of Wave Celerity and Wave Number

Observations of breaking wave fronts running over a submerged mound reveal that the part of wave front on top of the crest moves faster than the neighboring part of wave front on the side slopes, even though the water depth is shallower at the crest than on the side. The increase of wave speed is caused by the fact that the wave celerity is not only governed by the water depth but also affected by the wave amplitude; *i.e.*, a finite amplitude effect. Because the wave refraction by local topography is controlled by the spatial variation of wave celerity, a correct representation of wave celerity is required for appropriate evaluation of wave transformations. The finite amplitude effect on wave celerity was approximated by Goda (1995) as in the following empirical formulation:

$$c = \begin{cases} c_A \left[1 + \dfrac{3}{8}\left(\dfrac{H}{h}\right)^2\right]^{1/2} & : H < 2h \\[3mm] c_A \left[1 + \dfrac{3}{4}\left(\dfrac{H}{h}\right)\right]^{1/2} & : H \geq 2h \end{cases} \qquad (3)$$

where c_A denotes the wave celerity by the small amplitude wave theory, H the wave height, and h the local water depth.

The upper expression in the right-hand side of Eq. 3 was formulated in analogy of the phase velocity of the 3rd order Stokes waves. The lower expression was set to make a smooth transition across the boundary of $H = 2h$. The wave numbers k_x and k_y have been adjusted by dividing them with this rate of wave celerity increase. However, the group velocity c_g has been kept the same as that given by the small amplitude wave theory

Formulation of Wave Attenuation Function

The wave attenuation function f'_D was given the following form as discussed by Goda (1995):

$$f'_D = \begin{cases} 0 & : H < \gamma h \\[2mm] \dfrac{K}{2h}\left[\left(\dfrac{H}{\gamma h}\right)^2 - 1\right]^{1/2} & : H \geq \gamma h \end{cases} \qquad (4)$$

The constant K in Eq. 4 represents the relative rate of wave energy decay by breaking. It was given the value of $K = 0.125$ which yielded best agreement with the results of previous model tests. As for γ, which is the ratio of wave height to water depth at breaking, the present study sets its value according to the following breaker index by Goda (1974):

$$\gamma = 0.17\frac{L_0}{h}\left\{1 - \exp\left[-\frac{1.5\pi h}{L_0}(1 + 15\tan^{4/3}\theta)\right]\right\} \qquad (5)$$

where L_0 is the deepwater wavelength and θ represents the angle of inclination of bottom slope from the horizon. In the present study, the $\tan\theta$ was set at $1/30$ throughout the computational area inclusive of the submerged crests of reef systems, for the sake of simplicity.

Computation of Irregular Wave Heights

Though the numerical scheme of the parabolic equation has been developed for regular waves, the effect of wave irregularity can be taken into account by superposing the results of regular wave analysis for multiple levels of wave heights but with the same wave period. Individual wave heights are assumed to follow the Rayleigh distribution, and the range of wave height distribution is divided into N segments with the equal probability of appearance. The wave height representing

each segment is assigned as

$$H_m = 0.706(H_{1/3})_I \left[\ln \frac{2N}{2m - 1}\right]^{1/2} \qquad (6)$$

where N is the number of representative wave components and m is an integer from 1 to N ($m = 1$ yields the largest height and $m = 30$ the smallest). In the present study, $N = 30$ was employed. The results of the computations of N components at a given grid point were summed up to calculate the representative heights of irregular waves. By summing up the upper one-third components and multiplying it with the probability of appearance, the significant height $H_{1/3}$ is obtained, while the summation of the whole components yields the mean height $\overline{H}$.

Computation of Radiation Stresses

For each component of regular waves, the radiation stresses S_{xx}, S_{xy}, and S_{yy} are computed at each grid point from the results of wave amplitude and direction. The results of the 30 components are summed up to yield the overall radiation stresses, which provide the steady state input for computation of wave setup and wave-induced currents. As the radiation stress is proportional to the wave energy density, the overall radiation stress in the present study is an energy-averaged one.

Numerical Analysis of Wave Setup and Wave-Induced Currents

Governing Equations

The wave-induced currents and water level change are simulated by solving the continuity and momentum equations for long waves with the input of radiation stresses computed from the wave deformation analysis. The continuity equation is expressed as

$$\frac{\partial \zeta}{\partial t} + \frac{\partial U(h + \zeta)}{\partial x} + \frac{\partial V(h + \zeta)}{\partial y} = 0 \qquad (7)$$

where ζ denotes the amount of water level change, and U and V represent the cross-shore and longshore components of depth-integrated current speeds, respectively. The equations of motions are described as

$$\frac{\partial U}{\partial t} + U\frac{\partial U}{\partial x} + V\frac{\partial U}{\partial y} + F_x - M_x + R_x + g\frac{\partial \zeta}{\partial x} = 0 \qquad (8)$$

$$\frac{\partial V}{\partial t} + U\frac{\partial V}{\partial x} + V\frac{\partial V}{\partial y} + F_y - M_y + R_y + g\frac{\partial \zeta}{\partial y} = 0 \qquad (9)$$

where F represents the friction terms, M the horizontal mixing terms, R the gradients of radiation stresses, and g the acceleration of gravity.

The friction terms are evaluated with the friction coefficient $C_f = 0.01$ by using the vector-sum velocity of wave-induced currents and orbital velocity at the bottom. The horizontal mixing terms are calculated with the dimensionless

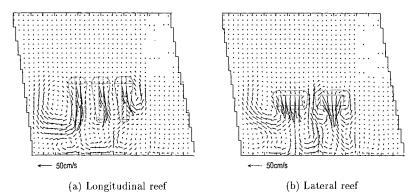constant $N = 0.016$ after Longuet-Higgins (1970).
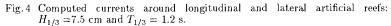
Computational Procedures

The governing equations are solved with the finite difference scheme. The central difference is employed for spatial grids and the forward differences are used for time steps. The grid size is the same as that for wave field, and the time step was set at $\Delta t = 0.01s$.

Computation starts from the condition of rest with the input of spatially-distributed radiation stresses, which are adjusted to increase gradually to the full magnitude to avoid computational instability. As computation progresses, the changes in water level and wave-induced currents approach to the equilibrium state. In the present study, the computation was stopped when the maximum value, throughout the computation area, of the velocity difference from the preceding time step became equal to 0.001 cm/s or less. Because this condition was quite strict compared with conventional computations of wave-induced currents, one run of computation required 5,000 to 10,000 time steps to yield the final results.

Examples of Wave-Induced Current Computation

Figure 4 exhibits the computed results of wave-induced currents around the reef systems for irregular waves with $H_{1/3}$ =7.5 cm and $T_{1/3}$ =1.2 for both the longitudinal and lateral reefs. Strong onshore currents are generated on top of reef units as expected. Rip currents between reef units are stronger for the lateral reef than for the longitudinal reef. Counterclockwise vortices at the left sides of both figures are probably the results of insufficient calibration of side boundary conditions in numerical works.

| (a) Longitudinal reef | (b) Lateral reef |

Fig. 4 Computed currents around longitudinal and lateral artificial reefs: $H_{1/3}$ =7.5 cm and $T_{1/3}$ = 1.2 s.

Wave Heights and Currents around Longitudinal Reef System

Significant wave heights measured in the physical models are compared with the results of numerical computations in Figs. 5 and 6. The former is for waves $H_{1/3}$ =5.5 cm and $T_{1/3}$ = 1.6 s, and the latter is for waves $H_{1/3}$ =7.5 cm and $T_{1/3}$ = 1.2 s. The left drawings show the cross-shore variations of wave heights along the line y =2.5 m (middle line between the first and second reef units), while the right drawings depict the longshore variations along the line x =4.75 m (just behind the reef units).
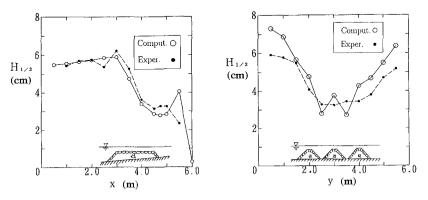

Fig. 5 Comparison of measured and computed wave heights around the longitudinal reef system for waves of $H_{1/3}$ =5.5 cm and $T_{1/3}$ = 1.6 s: the cross-shore variation along y =2.5 m in the left and the longshore variation along x =4.75 m in the right.
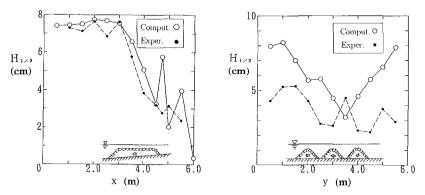

Fig. 6 Comparison of measured and computed wave heights around the longitudinal reef system for waves of $H_{1/3}$ =7.5 cm and $T_{1/3}$ = 1.2 s: the cross-shore variation along y =2.5 m in the left and the longshore variation along x =4.75 m in the right.

Numerical computation generally yields the wave heights almost in agreement with the measurements. Exception is the longshore variation of Fig. 6 in the left drawing, in which numerical computation overpredicts wave heights. Because the local water depth along the line $x = 4.75$ m is $h = 6.25$ cm, the significant wave height by random wave breaking should be about 5.3 cm according to the random wave breaking model by Goda (1975). However, computation predicts the wave height up to 8 cm.

The discrepancy is due to the use of a simple technique of representing irregular waves with segments of wave heights as determined by Eq. 6. Each component of waves is treated as regular waves, and the wave height after breaking eventually becomes $H = \gamma h$ regardless of incident wave heights. The original Rayleigh distribution of wave heights is transformed to have an upper cutoff at $H = \gamma h$. Thus the wave height in very shallow water approaches to the breaker height of regular waves.

Comparison of the measured and computed wave-induced currents are shown in Fig. 7. On top of the reef crests, strong onshore currents were visually observed, but they could not be confirmed by measurements, because the current meter emerged at the troughs of large waves and could not produce reliable records. The current patterns and velocities of measurements and computations are quite similar except for the counterclockwise vortices in the left which are predicted by computation but not observed in the measurements.
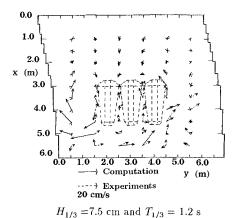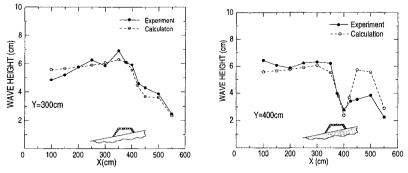

$H_{1/3} = 7.5$ cm and $T_{1/3} = 1.2$ s

Fig. 7   Measured and computed wave-induced currents around the longitudinal reef.

Wave Heights and Currents around Lateral Reef System

The distributions of wave heights around the lateral reef system are exhibited in Figs. 8 and 9. The cross-shore wave height variations are shown in Fig. 8 for waves with $H_{1/3} = 5.5$ cm and $T_{1/3} = 1.6$ s. The line $y = 3.0$ m at the middle of the two reef units and the line $y = 4.0$ m being off the central axis of the

second unit by 0.1 m were chosen for demonstration and shown in the left and right drawings, respectively. In the area between the reef units, the computed and measured significant wave heights are in good agreement. On top of the reef crest, wave heights decrease rapidly and the computation can simulate the wave decay quite well. However, in the area behind the reef along this section, the computation gives the wave height much higher than the measurement. This height corresponds to the breaker height of regular waves, owing to the use of a simple representation of irregular waves by Eq. 6 as discussed earlier.
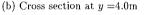

(a) Cross section at y =3.0 m   (b) Cross section at y =4.0m

Fig. 8 Cross-shore wave height variations around the lateral reef system: $H_{1/3}$ =5.5 cm and $T_{1/3}$ = 1.6 s.

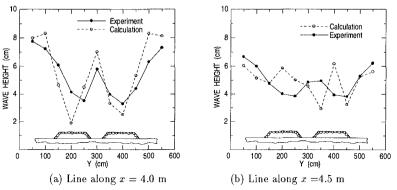(a) Line along x = 4.0 m   (b) Line along x =4.5 m

Fig. 9 Longshore wave height variations around the lateral reef system: $H_{1/3}$ =7.5 cm and $T_{1/3}$ = 1.2 s.

The longshore variations of wave heights are shown in Fig. 9 for waves with $H_{1/3}$ =7.5 cm and $T_{1/3}$ = 1.2 s. The line along x =4.0 m in the left is located slightly behind the rear tip of the crest, and the line along x =4.5 m in the right is located in the area of planar slope. Though computed wave heights exhibit

wider variations than the measured ones, they are approximately in agreement.

The strength of wave-induced currents around the lateral reef system is compared with that of the longitudinal system in Tables 1 and 2. Examples of currents by computation have been shown in Fig. 4. The maximum rip currents through the gap of reef units by model tests and numerical computation are listed in Table 1, and those of the maximum longshore currents are listed in Table 2.

Table 1 Maximum Rip Currents at the Gaps of Reef Units

$H_{1/3}$	$T_{1/3}$	Lateral Reefs		Longitudinal Reefs	
		experiments	computation	experiments	computation
5.5 cm	1.6 s	8.5 cm/s	13.2 cm	8.3 cm/s	10.5 cm/s
7.5 cm	1.2 s	12.0 cm/s	28.5 cm	11.4 cm/s	15.0 cm/s

Table 2 Maximum Longshore Currents behind the Reef Units

$H_{1/3}$	$T_{1/3}$	Lateral Reefs		Longitudinal Reefs	
		experiments	computation	experiments	computation
5.5 cm	1.6 s	10.1 cm/s	14.7 cm	11.8 cm/s	25.0 cm/s
7.5 cm	1.2 s	9.6 cm/s	19.8 cm	11.3 cm/s	22.5 cm/s

Numerical computation predicts stronger rip currents for lateral reefs and weaker longshore currents for a lateral reef system than for a longitudinal reef system. However, measurements did not record velocities as strong as those by computation, and differences between the two reef systems were not significant. A relatively small number of current measurement points might have been a reason that measurements could not detect the largest velocities around the reef system.

Discussion on Numerical Computation for Artificial Reef System

Figures 4 through 9 provide the basis for judging the accuracy and reliability of the numerical computation method employed in the present analysis. Admittedly it has several shortcomings, such as false current patterns and locally large wave heights in the area sheltered by the reef units.

One problem inherent to the numerical analysis around reef systems is the steep gradients at the front, sides, and rear slopes of reef units. Application of the mild slope equation as well as the parabolic equation to such a bathymetry violates the assumption of gradual variations of the physical quantities involved. Nevertheless, the parabolic equation by Hirakuchi and Maruyama (1986) can predict the wave height distribution relatively well. Wave irregularity has been incorporated simply by summing up the computational results for multiple levels of wave heights.

The merit of the parabolic equation is the fast speed in computation, because the spatial distribution of wave amplitude is directly solved. Computations of various reef layouts are done quickly and a best layout can be selected. A weak point in the present analysis is the difficulty in an appropriate evaluation of the wave decay function f_D' which would well behave on top of reef units as well as

in the rear area. The assessment of f'_D needs a calibration with laboratory data. The scale effect is a problem in model tests of artificial reefs, because the water depth at the reef crest is often quite small. Goda and Morinobu (1997) reported that a minimum water depth of 10 cm is required to correctly reproduce the wave breaking phenomenon on a trapezoidal step; a smaller water depth results in a smaller height-to-depth ratio at breaking.

Comparison of Prototype Lateral and Longitudinal Reef Systems

As the foregoing discussions were limited to the model reef systems, an examination of prototype structures is presented in the following.

A prototype situation is postulated as shown in Fig. 10. The sea bottom has the gradient of $1/20$ from the shoreline to the depth $h = 2$ m, $1/50$ from the depth $h = 2$ to 10 m, and 0 beyond 10 m. A lateral artificial reef system of two units ($a = 150$ m and $B = 40$ m) with the gap 50 m (at the crest level) is set at the location of $x = 280$ to 320 m in the water depth from $h = 4.5$ to 3.7 m. For comparison, a longitudinal artificial reef system with seven units ($a = 20$ m and $B = 65$ m) is set at the location of $x = 280$ to 345 m in the water depth from $h = 4.5$ to 3.2 m. The submergence depth is $h_c = 1.5$ m, the front and rear slopes have the gradient of $1/2$, and the side slopes has the gradient of $3/10$ for both the systems. The approximate volume of the lateral system is $64,000$ m^3, while the latter is $62,000$ m^3.
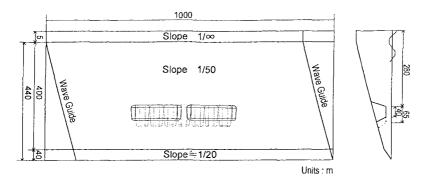

Fig. 10 Setup of computational area for lateral and longitudinal reef systems.

Figure 11 shows examples of computation of wave height distributions. The incident waves are unidirectional irregular waves with the height $H_{1/3} = 1.0$ and 3.0 m, the period $T_{1/3} = 8$ s, and the incident angle of $15°$. The top figures show the wave heights along the front edges of the both reef systems ($h = 4.5$ m), the center figures are for those along the middle line of the reefs ($h = 3.5$ m), and the bottom figures correspond to those along the rear edge of the longitudinal reef ($h = 2.5$ m).

As seen in Fig. 11, wave heights behind the longitudinal reef system are found to be lower than those behind the lateral system. Difference is prominent in the case of the small wave height $H_{1/3} = 1.0$ m. It is owing to the acceleration of wave breaking process by increase of wave height owing to the wave refraction effect at the heads of longitudinal reefs. Thus a longitudinal reef system is judged superior to a lateral reef system in the efficiency of energy dissipation when the crest submergence depth is the same.

In construction of prototype structures, a lateral reef system requires a minimum depth of 2 m or so owing to the limitation of the draft of working vessels. On the other hand, a longitudinal reef system can be constructed with the zero crest depth, because the crest width is small and a working vessel can reach out the crane arm to any location on the crest while mooring along the side slopes. Wave damping capacity of a longitudinal reef system can be further enhanced by setting the crest elevation as close to the low water level.
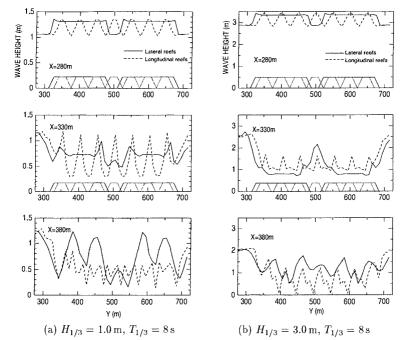

(a) $H_{1/3} = 1.0$ m, $T_{1/3} = 8$ s   (b) $H_{1/3} = 3.0$ m, $T_{1/3} = 8$ s

Fig. 11 Computed wave heights around the lateral and longitudinal reef systems

Conclusions

Major findings in the present studies are summarized as in the following:

1. A numerical scheme based on the parabolic equation for irregular waves demonstrated its capability to simulate the wave height distribution around

the lateral and longitudinal artificial reef systems. The capability was confirmed through comparison with 3-D model test data.

2. Wave-induced currents around the artificial reefs were approximately simulated by numerical computation, though further refinements are needed.

3. The newly-proposed longitudinal reef system has been shown more efficient in dissipating wave energy than the conventional lateral artificial reef system, because of incorporation of wave refraction effect.

4. Strong rip currents between the gap between the lateral units were predicted by computation, but model tests did not yield appreciable differences in current speeds between the longitudinal and lateral reef systems.

References

Goda, Y. (1974): New wave pressure formulae for composite breakwater, *Proc. 14th Int. Conf. on Coastal Engrg.*, Copenhagen, pp.1702-1720.

Goda, Y. (1975): Irregular wave deformation in the surf zone, *Coastal Engrg. in Japan*, JSCE, Vol. 18, pp.13-26.

Goda, Y. (1995): Wave damping characteristics of longitudinal reef system, *Advances in Coastal Structures and Breakwaters (Proc. of Conf.)* edited by J. E. Clifford, Thomas Telford Pub., London, pp.192-203.

Goda, Y. and K. Morinobu (1997): Breaking wave height on horizontal bed, *Proc. Combined Australasian Coastal Engrg. and Ports Conf.*, Christchurch, New Zealand, pp.953-958.

Hirakuchi, H. and K. Maruyama (1986): An extension of the parabolic equation for application to obliquely incident waves, *Proc. 33th Japanese Conf. on Coastal Engrg.*, pp.114-118 (*in Japanese*).

Longuet-Higgins, M. S. (1970): Longshore currents generated by obliquely incident sea waves, 2, *J. Geophys. Res.*, Vol. 75, No. 33, pp.6790-6801.